



HAL
open science

Inclusion complex vs. conjugation of hydrophobic photosensitizers with β -cyclodextrin: Improved disaggregation and photodynamic therapy efficacy against glioblastoma cells

Amina Ben Mihoub, Zahraa Youssef, Ludovic Colombeau, Valérie Jouan-Hureau, Philippe Arnoux, Céline Frochot, Régis Vanderesse, Samir Acherar

► To cite this version:

Amina Ben Mihoub, Zahraa Youssef, Ludovic Colombeau, Valérie Jouan-Hureau, Philippe Arnoux, et al.. Inclusion complex vs. conjugation of hydrophobic photosensitizers with β -cyclodextrin: Improved disaggregation and photodynamic therapy efficacy against glioblastoma cells. *Materials Science and Engineering: C*, 2020, 109, pp.110604. 10.1016/j.msec.2019.110604 . hal-02433562

HAL Id: hal-02433562

<https://hal.univ-lorraine.fr/hal-02433562v1>

Submitted on 21 Jul 2022

HAL is a multi-disciplinary open access archive for the deposit and dissemination of scientific research documents, whether they are published or not. The documents may come from teaching and research institutions in France or abroad, or from public or private research centers.

L'archive ouverte pluridisciplinaire **HAL**, est destinée au dépôt et à la diffusion de documents scientifiques de niveau recherche, publiés ou non, émanant des établissements d'enseignement et de recherche français ou étrangers, des laboratoires publics ou privés.



Distributed under a Creative Commons Attribution - NonCommercial 4.0 International License

1 Inclusion complex vs. conjugation of hydrophobic 2 photosensitizers with β -cyclodextrin: Improved 3 disaggregation and photodynamic therapy efficacy 4 against glioblastoma cells

5 Amina Ben Mihoub,^{a,b} Zahraa Youssef,^c Ludovic Colombeau,^{a,c} Valérie Jouan-Hureaux,^d Philippe
6 Arnoux,^c Céline Frochot,^c Régis Vanderesse,^a and Samir Acherar*^a

7 ^a Université de Lorraine, CNRS, LCPM, F-54000 Nancy, France

8 ^b Laboratory of Physical Chemistry of Materials (LPCM), Faculty of Sciences, (UATL) BP 37G Laghouat
9 03000, Algeria

10 ^c Université de Lorraine, CNRS, LRGP, F-54000 Nancy, France

11 ^d Université de Lorraine, CNRS, CRAN, F-54000 Nancy, France

12 * Corresponding Author: samir.acherar@univ-lorraine.fr

13 Abstract

14 Self-aggregation of hydrophobic porphyrin-based photosensitizers (PSs) in aqueous biological
15 environment decreases their bioavailability and *in vivo* therapeutic efficacy, which hampers their clinical
16 use in photodynamic therapy (PDT). In the current study, we explore three new supramolecular systems
17 based of hydrophobic PSs (*i.e.* 5,10,15,20-tetrakis(3-hydroxyphenyl)porphyrin (*m*THPP) or 5-(4-
18 carboxyphenyl)-10,15,20-triphenylporphyrin (PICOOH)) non-covalently or covalently attached to β -CD.
19 The two non-covalent solid inclusion complexes $(\beta\text{-CD})_2/m\text{THPP}$ and $[(\beta\text{-CD})/\text{PICOOH}]_4$ are prepared
20 by a new co-precipitation@lyophilization combined method and the covalent conjugate $\beta\text{-CD-P1}$ by click
21 chemistry. The binding type effect and effectiveness on the disaggregation in aqueous medium and *in*
22 *vitro* PDT efficacy against glioblastoma cancer cells of PSs are investigated for the three $\beta\text{-CD}/\text{PS}$
23 systems. The findings reveal a remarkable improvement of the disaggregation and *in vitro* PDT activity of
24 these $\beta\text{-CD}/\text{PS}$ systems compared to the free PSs, except for $[(\beta\text{-CD})/\text{PICOOH}]_4$ inclusion complex

25 caused by J-type self-aggregation of the inclusion complex in tetrameric form. β -CD-P1 conjugate shows
26 the higher *in vitro* PDT efficacy compared to the other β -CD/PS systems. Overall, the results indicate that
27 the disaggregation in aqueous medium and *in vitro* PDT activity of hydrophobic PSs can be improved by
28 their binding to β -CD and the covalent binding is the best approach.

29 **Keywords:** β -Cyclodextrin, Photosensitizer, Inclusion complex, Conjugation, Disaggregation,
30 Photodynamic therapy, Glioblastoma.

31 **Corresponding Author:** E-mail: samir.acherar@univ-lorraine.fr. Phone: +33 037-274-3687.

32 1. Introduction

33 Photodynamic therapy (PDT) is a minimally invasive cancer treatment involving the generation of
34 reactive oxygen species (ROS), particularly singlet oxygen ($^1\text{O}_2$), which causes cell apoptosis and
35 necrosis [1]. ROS generation is based on the light photoactivation of a photosensitizer (PS) at a particular
36 wavelength followed by its interaction with molecular oxygen. However, one of the major drawbacks of
37 PDT is the poor water solubility of PSs, limiting their clinical usefulness. The most effective PSs for PDT
38 are hydrophobic molecules which typically present a strong propensity to self-aggregate in water,
39 resulting in lowered $^1\text{O}_2$ generation (*i.e* diminution of the PDT efficacy) and administration difficulties
40 [2].

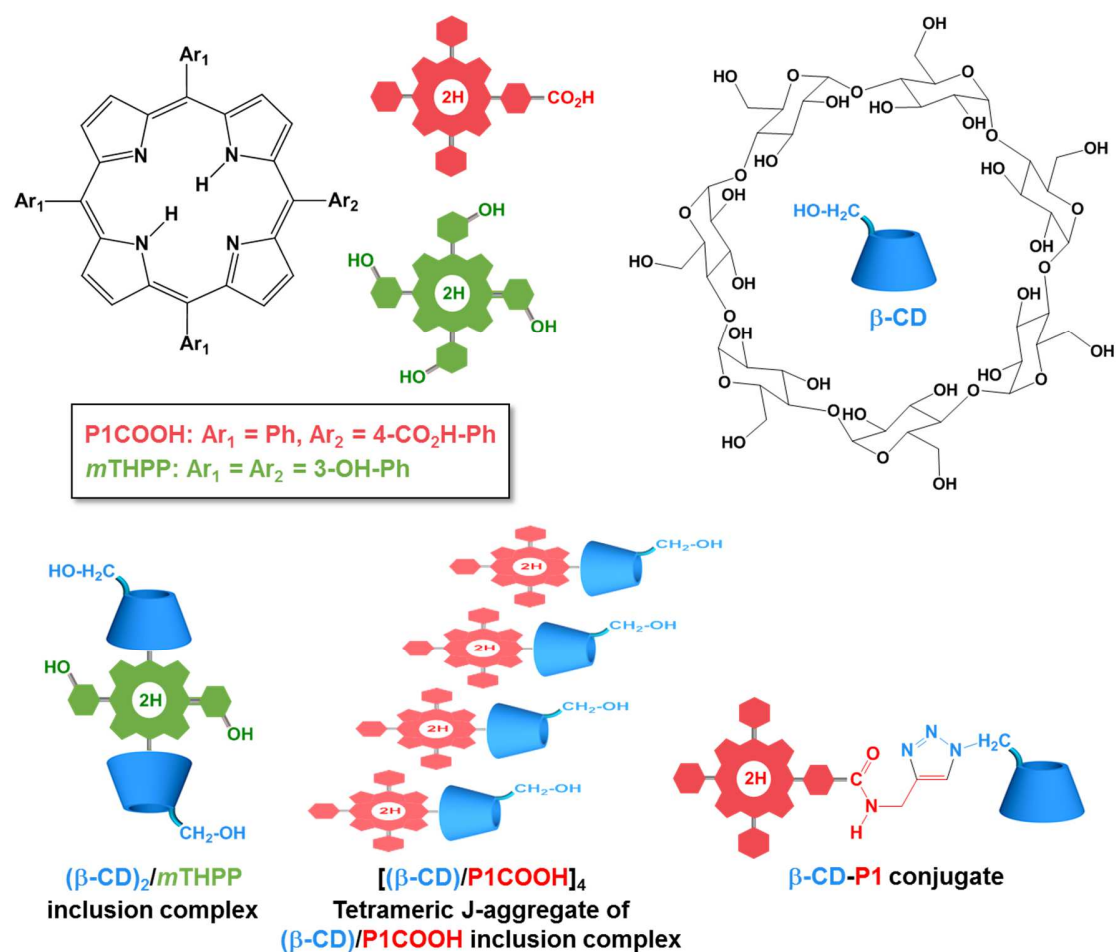
41 The emergence of the nanotechnology has deeply affected various biomedicine areas, including PDT [3].
42 Among the various branches of nanotechnology, the use of biocompatible nanovectors for PSs
43 administration has paved the way for a significant improvement in their bioavailability, biodistribution
44 and PDT efficacy [4-6]. Cyclodextrins (CDs) are by far one of the most promising biocompatible
45 nanovectors of PSs [7,8] thanks to their water-soluble, biocompatible, crystalline and non-hygroscopic
46 properties. CDs are a family of natural glucopyranose-based cyclic oligosaccharides, containing a
47 relatively hydrophobic central cavity that can be used to form reversibly and selectively host-guest
48 inclusion complexes with various guest molecules in aqueous media [9-14]. Inclusion complexation (non-
49 covalent binding) or conjugation (covalent binding) of PSs with CDs lead to a significant improvement in
50 water solubility, ROS production and PDT efficacy of PSs against cancer cells [15-19].

51

52 In this context, the present study aims to compare the effect and effectiveness of the binding type (non-
53 covalent vs. covalent) of β -CD with hydrophobic PSs on the disaggregation in aqueous medium and *in*
54 *vitro* PDT efficacy of PSs.

55 Our starting hypothesis is that a covalent link (β -CD-PS conjugate) must be more stable than non-
56 covalent link (β -CD/PS inclusion complex) in aqueous medium because the complex formation and
57 dissociation are dynamic equilibrium processes while the conjugate forms unbreakable covalent bond
58 between β -CD and PS. Thus, we assume that the covalent link should give the better effect on PSs in
59 terms of disaggregation in aqueous medium and *in vitro* PDT efficacy against glioblastoma cells.

60 To answer to the above hypothesis, we explore three new supramolecular systems based of hydrophobic
61 PSs (*i.e.* 5,10,15,20-tetrakis(3-hydroxyphenyl)porphyrin (*m*THPP) or 5-(4-carboxyphenyl)-10,15,20-
62 triphenylporphyrin (P1COOH)) non-covalently or covalently attached to β -CD. These supramolecular
63 systems consist of two non-covalent solid inclusion complexes ($(\beta\text{-CD})_2/m\text{THPP}$ and $[(\beta\text{-}$
64 $\text{CD})/P1\text{COOH}]_4$) and one covalent conjugate ($\beta\text{-CD-P1}$) (Fig.1). The solid inclusion complexes are
65 prepared by co-precipitation@lyophilization combined method and characterized by ^1H NMR, FTIR,
66 XRD, TG-DTA techniques. The conjugate $\beta\text{-CD-P1}$ is synthesized using Copper-Catalyzed Azide-
67 Alkyne Cycloaddition (CuAAC) click chemistry and characterized by NMR (^1H , ^{13}C , 2D HSQC and 2D
68 HMBC) and HRMS techniques. The binding type effect and effectiveness of the $\beta\text{-CD/PS}$ systems on the
69 disaggregation in aqueous medium and *in vitro* PDT activity against glioblastoma U87 and U251 cells
70 cancer cells are investigated and compared.



71

72 **Fig. 1.** Chemical structures of *m*THPP, P1COOH and β -CD, and schematic illustration of the three
 73 studied β -CD/PS systems.

74 2. Materials and methods

75 2.1. Chemicals

76 All chemicals were purchased as the highest purity commercially available and used without further
 77 purifications. β -CD was purchased from Sigma-Aldrich and photosensitizers (*m*THPP and P1COOH)
 78 from PorphyrChem Company. All reactions involving porphyrin compounds were performed in the dark
 79 by protecting the reactors and other glassware with aluminium foil. Bioassays were evaluated on human
 80 glioblastoma U251 (Sigma-Aldrich) and U87 MG (ATCC® HTB-14™) cell lines.

81 2.2. Characterization

82 Reactions were monitored by thin-layer chromatography (TLC) using aluminium-backed silica gel plates
83 (Macharey-Nagel ALUGRAM® SIL > G/UV254). TLC spots were viewed under ultraviolet light (256
84 nm). Porphyrin compounds purifications were performed either by flash chromatography using Geduran
85 60 H Silica Gel (63-200 mesh) or by reverse phase high performance liquid chromatography (HPLC)
86 (C18 column) using methanol/water or acetonitrile/water (v/v) gradients (from 10/90 to 100/0 in 25 min,
87 then 100/0 for 15 min). Infrared spectra were recorded with an attenuated total reflectance Fourier
88 transform infrared (FTIR) Bruker ALPHA spectrophotometer with a wavenumber between 400 and 4000
89 cm^{-1} . Ultraviolet-Visible (UV-vis) absorption spectra were measured on a Shimadzu UV-3600 double-
90 beam UV-vis spectrophotometer. Fluorescence spectra were recorded on a Fluorolog-3
91 spectrofluorometer FL3-222. Powder X-ray diffraction (XRD) measurements were performed using a
92 Panalytical X'Pert Pro diffractometer equipped with a Cu tube, a Ge (111) incident beam monochromator
93 ($\lambda = 1,5406 \text{ \AA}$) and an X'Celerator detector. Data collections were recorded in the $3\text{-}70^\circ$ scattering angle
94 range with a pitch of 0.0167° for 90 min. Thermogravimetric (TG) and differential thermal (DTA)
95 analyses were performed on a Mettler Toledo TGA/DSC1 Star System under N_2 atmosphere at a heating
96 rate of $10^\circ\text{C}/\text{min}$ in a temperature range of $30\text{-}900^\circ\text{C}$. ^1H and ^{13}C NMR spectra were recorded on a
97 Bruker Advance 300 MHz spectrophotometer. The spectra were recorded in $\text{DMSO-}d_6$ at room
98 temperature ($T = 298 \text{ K}$) using residual DMSO peaks ($\delta = 2.5 \text{ ppm}$ for ^1H NMR and $\delta = 39.5 \text{ ppm}$ for ^{13}C
99 NMR). Chemical shifts (δ) were reported in parts per million (ppm). Coupling constants (J) were given in
100 hertz (Hz) and the multiplicity was defined as s for singlet, t for triplet, m for multiplet, br for broad, Pyr
101 for pyrrole, Ar for aromatic or combinations thereof. Electrospray ionization high resolution mass
102 spectrum (ESI-HRMS) was recorded on a Bruker MicrOTOF-Q HR spectrometer.

103 2.3. *Synthesis of $(\beta\text{-CD})_n/\text{PS}$ inclusion complexes*

104 2.3.1. *Stoichiometry (n) and association constant (K_a) determination*

105 Firstly, the stoichiometry (n) was determined using Job's method [20]. In brief, stock solutions of
106 equimolar concentrations ($c = 10 \mu\text{M}$) of $\beta\text{-CD}$ (in MeOH/milli-Q water or THF/milli-Q water, 50/50,
107 v/v) and PS ($m\text{THPP}$ in MeOH/milli-Q water or P1COOH in THF/milli-Q water, 50/50, v/v) were
108 prepared. These solutions of $\beta\text{-CD}$ and PS were mixed at various volumes to provide different samples
109 having a constant total concentration of $10 \mu\text{M}$, a constant total volume of 5 mL and a molar ratio of PS
110 varying from 0 to 1. The solutions were mixed in a thermostatic mixer at 30°C , 100 rpm for 24 h.
111 Finally, the absorbance for all sample were measured ($\lambda_{\text{exc}} = 415 \text{ nm}$) and the absorbance differences ($A\text{-}$
112 A_0) were calculated and plotted against the mole fractions (r). The n value for the studied $(\beta\text{-CD})_n/\text{PS}$

113 inclusion complex was determined with the r value at the maximum of $(A-A_0)$ on the Job curve using
114 Eq.1.

$$115 \quad r = \frac{[PS]_T}{([PS]_T + [\beta\text{-CD}]_T)} = \frac{1}{1+n} \quad \text{Eq. 1}$$

116 where r was the mole fraction, $[PS]_T$ and $[\beta\text{-CD}]_T$ were the total concentrations of PS and $\beta\text{-CD}$ in
117 samples, and n was the complexation order.

118 Secondly, the association constant (K_a) was calculated using Benesi-Hildebrand's method [21]. A 1 mL
119 solution of PS (*m*THPP in MeOH or PICOOH in THF, $c = 25 \mu\text{M}$) was added to a 9 mL solution of $\beta\text{-CD}$
120 at various concentrations ($c = 2 \text{ mM}$ to 20 mM). The different samples were mixed in a thermostatic
121 mixer at $30 \text{ }^\circ\text{C}$, 100 rpm for 30 min. Finally, the absorbance for all sample were measured ($\lambda_{\text{exc}} = 415 \text{ nm}$)
122 and the absorbance differences $(1/A-A_0)$ were calculated and plotted against the concentrations $([\beta\text{-CD}]_0)^n$. The K_a value for the studied $(\beta\text{-CD})_n/\text{PS}$ inclusion complex was determined with the linear
123 relationship between $[1/(A-A_0)]$ and $([\beta\text{-CD}]_0)^n$ on the Benesi-Hildebrand curve using Eq.2.
124

$$125 \quad \frac{1}{(A-A_0)} = \left[\frac{1}{K_a} \times \frac{1}{(k \times Q \times [PS]_0)} \times \frac{1}{([\beta\text{-CD}]_0)^n} \right] + \frac{1}{(k \times Q \times [PS]_0)} \quad \text{Eq. 2}$$

126 where $A-A_0$ was the difference between the PS's absorbance values in the presence (A) and in the
127 absence (A_0) of $\beta\text{-CD}$, K_a was the association constant, k and Q were constants, $[PS]_0$ and $[\beta\text{-CD}]_0$ were
128 the initial concentrations of PS and $\beta\text{-CD}$ in samples, and n was the complexation order.

129 2.3.2. Solid $(\beta\text{-CD})_n/\text{PS}$ inclusion complexes

130 Solid $(\beta\text{-CD})_n/\text{PS}$ inclusion complexes were prepared using new approach by combining co-precipitation
131 and lyophilization methods. In brief, equimolar solution of *m*THPP (or PICOOH) in MeOH (or THF)
132 (0.2 mol , $c = 20 \text{ mM}$) was added dropwise at room temperature to a stirred solution of the equimolar
133 aqueous solution of $\beta\text{-CD}$ (0.2 mol , $c = 20 \text{ mM}$ in milli-Q water). The reaction mixture was warmed to
134 $60\text{-}70 \text{ }^\circ\text{C}$, allowed to stir for 5 h in the dark and the organic solvent was removed under vacuum. The
135 reaction mixture was diluted in milli-Q water and filtered through a $0.45 \mu\text{m}$ filter to remove the excess of
136 poorly water-soluble PS. The resulted filtrates were lyophilized at $-80 \text{ }^\circ\text{C}$ overnight in the dark and then
137 stored at $4 \text{ }^\circ\text{C}$ protected from light.

138 The $\beta\text{-CD}+\text{PS}$ physical mixtures were prepared by grinding equimolar amounts of PS and $\beta\text{-CD}$ using a
139 mortar until the obtaining of homogeneous mixtures.

140 2.4. Synthesis of $\beta\text{-CD-P1}$ conjugate

141 Porphyrin derivatives **1-2** were prepared in 96 % and 100 % yield, respectively, according to the protocol
142 previously described by our team [22].

143 2.4.1. Mono-6-(*p*-tolylsulfonyl)- β -cyclodextrin, **3**

144 β -CD derivative **3** was prepared using the protocol previously described by our team [23] with slight
145 modifications. β -CD (5.0 g, 4.40 mmol, 1 equiv) was dissolved in NaOH 10 wt. % solution (70 mL) and
146 left at 4 °C overnight. TsCl (5.0 g, 26.2 mmol, 6 equiv) was added in three equal portions to the β -CD
147 solution at 0 °C under vigorous stirring. 5 h later, the resulted mixture was purified by filtration the
148 resulted mixture was purified by filtration on Celite[®] through a fritted-glass funnel with 3 μ m frit
149 porosity. The filtrate was precipitated at 0-5 °C by adjusting the pH to 1-2 with concentrated HCl
150 solution and stored overnight at 4 °C. The precipitate was then filtered under vacuum, recrystallized three
151 times in hot ultra-pure water and dried overnight at 50 °C to provide **3** as a white powder. The
152 characterization of **3** is in agreement with those previously described in the literature [24]. ¹H NMR (300
153 MHz, DMSO-*d*₆) δ = 2.0 (s, 3H, CH₃ tosyl), 2.93-3.42 (m, 14 H, H4 and H2), 3.43-3.83 (m, 28H, H3, H5
154 and H6), 4.22-4.42 (m, 6H, OH6), 4.75 (br s, 1H, H1), 4.83 (br s, 6H, H1), 5.45-5.95 (br s, 14H, OH2
155 and OH3), 7.43 (d, 2H, *J* = 8.1 Hz, H9), 7.74 (d, 2H, *J* = 8.1 Hz, H8).

156 2.4.2. β -CD-P1 conjugate

157 β -CD derivative **4** was prepared in 96 % yield according to the protocol previously described in the
158 literature [24]. CuSO₄·5H₂O (0.1 equiv) and sodium ascorbate (0.5 equiv) were successively added to an
159 equimolar mixture of **2** and **4** (0.1 mmol, 1 equiv) in H₂O/THF (4/5, v/v, 5 mL). The mixture was refluxed
160 under vigorous stirring at 40 °C for 5 h in the dark. The reaction mixture was then cooled to room
161 temperature and washed with milli-Q water (3 x 20 mL), dried over MgSO₄, and concentrated under
162 reduced pressure. The crude product was purified by preparative HPLC to finally give a green powder of
163 the β -CD-P1 conjugate. ¹H NMR (300 MHz, DMSO-*d*₆) δ = -2.92 (s, 2H, 2 NH pyr), 3.16-3.85 (m,
164 overlap with HDO, 28H, 7 H2, 7 H3, 7 H4, 7 H5 and 14 H6), 4.05-4.62 (m, 7 OH6), 4.70 (br s, 2H, CH₂-
165 NH), 4.83 (br s, 6H, H1), 5.10 (br s, 1H, H1), 5.74 (br s, 14H, 7 OH2 and 7 OH3), 7.72-7.92 (m, 9H, H
166 Ar), 8.06 (s, 1H, CH triazole), 8.15-8.30 (m, 8H, H Ar), 8.32 (s, 2H, H Ar), 8.84 (s, 8H, H β pyr), 9.34 (t,
167 1H, *J* = 5.7 Hz, NH amide). ¹³C NMR (75 MHz, DMSO-*d*₆) δ = 35.0 (CH₂-NH), 59.9 (C₆), 72.0 (C2, C3
168 or C5), 72, 4 (C2, C3 or C5), 73.0 (C2, C3 or C5), 81.5 (C4), 101.9 (C1), 119.0 (C Ar), 120.1 (C Ar),
169 125.9 (CH triazole), 126.0 (CH Ar), 128.1 (CH Ar), 132.3 (CH β), 134.2 (CH Ar), 141.1 (C Ar), 144.1 (C

170 Ar), 144.6 (C triazole), 157.8 (C Ar), 166.3 (C=O). HRMS calculated for C₉₀H₁₀₂N₈O₃₅ [M+2H]^{+/2} m/z
171 928.8243; found 928.8271 (see Supporting Information, Figs. S1-S5).

172 2.5. Disaggregation study in aqueous medium

173 A fixed concentration of PS (*m*THPP or P1COOH, *c* = 2 μM) was used in the disaggregation study and
174 prepared by dissolution in a minimum of organic solvent (MeOH for *m*THPP and THF for P1COOH)
175 followed by dilution in milli-Q water. A 0.5 mL solution of PS was added to a 4.5 mL aqueous solution of
176 β-CD in milli-Q water at various concentrations. The resulted PS+β-CD solutions were warmed to 40 °C
177 and stirred for 30 min. The UV-vis absorption and fluorescence emission spectra were then recorded and
178 compared.

179 2.6. Binding type effect on PSs disaggregation in aqueous medium

180 The binding type effect of β-CD on the disaggregation in aqueous medium of *m*THPP and P1COOH in
181 the different β-CD/PS systems was studied by comparing their UV-vis, fluorescence and ¹O₂
182 luminescence spectra to those of free PSs in the same conditions. Briefly, aqueous solutions were
183 prepared by direct dissolution of each product in D₂O ((β-CD)₂/*m*THPP and [(β-CD)/P1COOH]₄) or by
184 dissolution in a minimum of DMSO followed by dilution in D₂O (β-CD-P1, *m*THPP and P1COOH). The
185 UV-vis absorption and fluorescence emission spectra were recorded at 200-800 nm and 600-800 nm
186 wavelength ranges, respectively. Fluorescence (φ_f) and singlet oxygen (φ_Δ) quantum yields were
187 determined using tetraphenyl porphyrin (TPP) solution in toluene as fluorescence standard (φ_f = 0.11)
188 [25] and Rose Bengal solution in D₂O as ¹O₂ reference (φ_Δ = 0.76) [26]. The absorbance value at the
189 excitation wavelength of the reference and the sample solutions were set around 0.2.

190 2.7. In vitro PDT activity

191 2.7.1. Cell culture conditions

192 Human glioblastoma U251 or U87 cells were cultured in DMEM (Dulbecco's Modified Eagle Medium)
193 supplemented with sodium pyruvate (1.5 mM) and vitamins MEM AA, MEM NE AA, L-Ser (14 μg/mL),
194 L-asp (25 μg/mL), L-Glu (2.5 mM), penicillin (100 U/mL), streptomycin (100 μg/mL) and 20 % fetal calf
195 serum (FCS) under standard cell culture conditions at 37 °C in a humidified atmosphere (80 %)
196 containing 5 % CO₂.

197 2.7.2. *In vitro* photodynamic activity

198 The dark cytotoxicity and phototoxicity of tested compounds (β -CD/PS systems, free PSs and β -CD) were
199 performed on human glioblastoma U87 and U251 cells after incubation in the dark (dark cytotoxicity) or
200 after exposure to light (phototoxicity). Cell viability was determined by measuring the activity of live cell
201 mitochondrial dehydrogenases (MTT assay) as previously described [27]. Briefly, cancer cells were
202 seeded at 2×10^4 cells/cm². The stock solutions of the tested compounds were prepared in HBSS (Hank's
203 Balanced Salt Solution) (2 mg/mL) and then diluted to the required concentrations in the DMEM culture
204 medium. Free *m*THPP, free P1COOH and β -CD-P1 conjugate were first dissolved in a minimum of
205 DMSO and the resulted solutions were diluted in the DMEM culture medium (it is important to note that
206 the concentration of the final DMSO not exceeded 0.25 %). After 48 h, the initial culture medium was
207 removed and the cancer cells were treated with each compound separately at a final PS concentration of 1,
208 2 and 3 μ M for U87 cells, and treated only with β -CD-P1 conjugate at a final PS concentration of 1, 2, 3,
209 5, 10 and 20 μ M for U251 cells. The cells were incubated in the dark for another 24 h. The cancer cells
210 were then washed three times with HBSS to remove the non-internalized tested compounds and a new
211 culture medium was added. In order to study the cytotoxic effect of the tested compounds, cancer cells
212 were kept in the dark. The photoinduced toxicity of these tested compounds was estimated by exposing
213 the cells to light (4.54 mW/cm², fluence 10 J/cm²) using a 652 nm diode laser system for 36 min. After
214 treatment, the cancer cells were incubated for an additional 24 h under standard culture conditions. The
215 viability of the cancer cells was evaluated using the MTT assay: 0.4 mg/mL of MTT (3-(4,5-
216 dimethylthiazol-2-yl)-2,5-diphenyltetrazolium bromide) was added to each well and the plates were then
217 incubated for 3 h at 37 °C. The old media was removed, and DMSO added to lyse the cells and dissolve
218 the formazan crystals that appeared in living cells. The absorbance of formazan was measured at
219 wavelength of 540/630 nm (Multiscan Ascent microplate reader). Cell viability was expressed in terms of
220 percentage of living cells vs. values obtained from untreated cells.

221 2.7.3. *Statistical analysis*

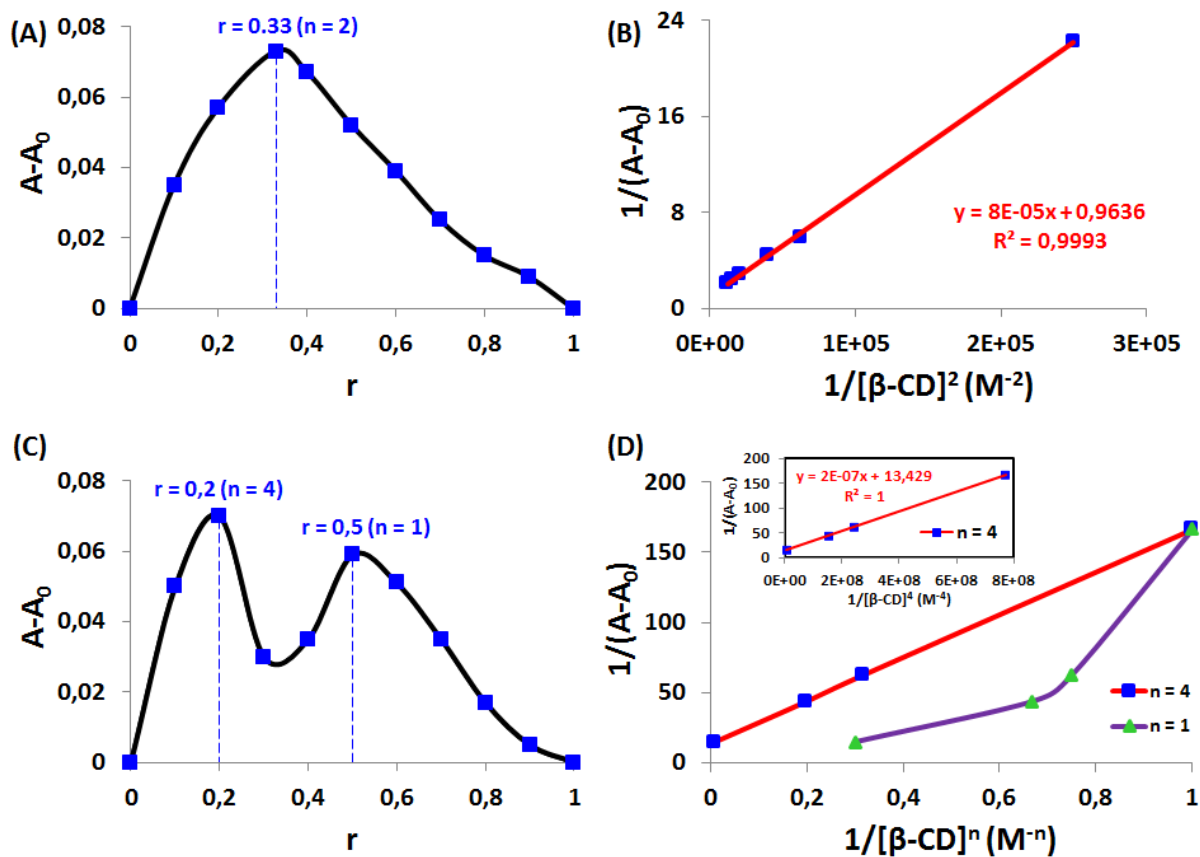
222 All *in vitro* experiments were realized in triplicate and the results were given as mean \pm standard
223 deviation (SD). Differences among groups were evaluated using variance analysis (Anova) followed by
224 Bonferroni test (GraphPad Prism 6.0 software). A value of $p < 0.05$ was considered as statistically
225 significant. * Vs. control cells, # vs. same compound at smaller concentration used.

226 3. Results and discussion

227 3.1. Stoichiometry (n) and association constant (K_a) determination

228 Prior to starting the synthesis of solid $(\beta\text{-CD})_n/\text{PS}$ inclusion complexes of $m\text{THPP}$ or PICOOH as guest
 229 and $\beta\text{-CD}$ as host, it is critical to determine both the stoichiometry (n) and the association constant (K_a) in
 230 the host-guest interaction. The classical methods employed to access the n and K_a values are Job's
 231 (continuous variation method) [20] and Benesi-Hildebrand's [21] methods using Eq.1 and Eq.2,
 232 respectively (see Section 2.3.1.).

233 For the $\beta\text{-CD}/m\text{THPP}$ system, the Job's continuous variation plot (Fig. 2A) reveals a maximum
 234 absorbance at the r value of 0.33 mole (at $\lambda = 415$ nm), corresponding to the n value of 2 from Eq. 1,
 235 indicating the formation of the $(\beta\text{-CD})_2/m\text{THPP}$ inclusion complex. The Benesi-Hildebrand plot (Fig. 2B)
 236 of measured absorbance $[1/(A-A_0)]$ at 415 nm vs. $([\beta\text{-CD}]_0)^2$ ($n = 2$) shows a linear relationship with a
 237 correlation (R^2) of 0.9993. By considering the 2:1 complex stoichiometry between $\beta\text{-CD}$ and $m\text{THPP}$, an
 238 association constant K_a of $1.2045 \cdot 10^4 \text{ M}^{-2}$ is determined from Eq. 2 and linear relationship between $[1/(A-$
 239 $A_0)]$ and $([\beta\text{-CD}]_0)^2$.



240

241 **Fig. 2.** (A) Job's and (B) Benesi-Hildebrand plots for complexation of *m*THPP with β -CD determined by
242 UV-vis absorption at 415 nm. (C) Job's and (D) Benesi-Hildebrand plots for complexation of PICOOH
243 with β -CD determined by UV-vis absorption at 415 nm.

244 For the β -CD/PICOOH system, the Job's continuous variation plot (Fig. 2C) shows some interesting
245 behaviour exhibiting two maxima at 1:1 and 4:1 stoichiometric ratios for the $(\beta\text{-CD})_n/\text{PICOOH}$ inclusion
246 complex. The Benesi-Hildebrand plot (Fig. 2D) reveals a linear relationship with a correlation (R^2) of 1
247 ($K_a = 3.723 \cdot 10^4 \text{ M}^{-4}$) for the 4:1 ratio only, which means that the inclusion complex involving 4 β -CDs is
248 the most stable. However, there is one major remaining question: Does the most stable 4:1 inclusion
249 complex from Job's plot is due to coordination of 4 β -CDs to the non-aggregated (*i.e.* monomeric species,
250 4:1 inclusion complex) as well as aggregated PICOOH (*i.e.* tetrameric species, self-aggregation of four
251 1:1 inclusion complexes). The answer to this question is given by the spectroscopic studies in aqueous
252 medium (see Sections 3.4. and 3.5.). In general, the inclusion complex with cyclodextrin does not affect
253 the UV-vis spectrum of small molecules but, in our case, the UV-vis spectrum of the inclusion complex
254 reveals a remarkable red shift of the Soret band indicating that a phenomenon of J-aggregation occurs in
255 this inclusion complex [28]. The aggregation phenomenon is also evidenced by the fluorescence emission
256 and $^1\text{O}_2$ luminescence quenching which is due to the self-aggregation of PSs in aqueous medium through
257 π - π stacking due to their hydrophobic and rigid planar structures [29-31]. All these data highlight the
258 presence of an inclusion complex with the 4 β -CDs in an aggregate form (*i.e.* tetrameric species, self-
259 aggregation of four 1:1 inclusion complexes, Fig. 1). It should be noted that the obtaining of a Job's plot
260 with two peaks is possible but quite rare. For example, P. Tau et al. in 2003 synthesized an inclusion
261 complex between β -CD and a tetrasubstituted zinc phthalocyanine (ZnPc) and obtained also a Job's plot
262 with 2 peaks [32]. The authors observed two maxima at inclusion ratios of about 2:1 and 4:1 (β -
263 CD:ZnPc), and came to the same conclusion as we did above, that the 2:1 corresponded to the
264 coordination of 2 β -CDs to the non-aggregated complex (*i.e.* monomeric species, 2:1 inclusion complex)
265 and 4:1 to the coordination of 4 β -CDs to the aggregated complex (*i.e.* dimeric species, self-aggregation
266 of two 2:1 inclusion complexes).

267 3.2. Synthesis and characterization of solid $(\beta\text{-CD})_n/\text{PS}$ inclusion complexes

268 With evidence now conclusive that inclusion complexes of *m*THPP or PICOOH as guest and β -CD as
269 host can be formed, preparation of solid $(\beta\text{-CD})_2/m\text{THPP}$ and $[(\beta\text{-CD})/\text{PICOOH}]_4$ inclusion complexes is
270 tackled for the first time using a new co-precipitation@lyophilization combined method. Solid inclusion

271 complexes formation is confirmed by studying the host-guest interactions with different experiments
 272 including ^1H NMR, FTIR, TG and DTA, and XRD.

273 ^1H NMR spectroscopy is one of the powerful experimental techniques for the investigation of the
 274 successful preparation of inclusion complexes [33]. The formation of a $(\beta\text{-CD})_n/\text{PS}$ inclusion complex is
 275 based on intermolecular interactions between PS and $\beta\text{-CD}$, resulting in changes in chemical shifts of $\beta\text{-CD}$.
 276 It is generally accepted, for $\beta\text{-CD}$, that the chemical shift values of H3 and H5 protons (located inside
 277 the cavity) are more variable than H2, H4 and H6 protons when the inclusion complex is formed [34,35].
 278 ^1H chemical shifts (δ) values for H1-H6 protons in $\beta\text{-CD}$ and solid $(\beta\text{-CD})_2/m\text{THPP}$ and $[(\beta\text{-CD})/$
 279 $\text{P1COOH}]_4$ inclusion complexes are given in Table 1 and confirm the successful preparation of both
 280 inclusion complexes.

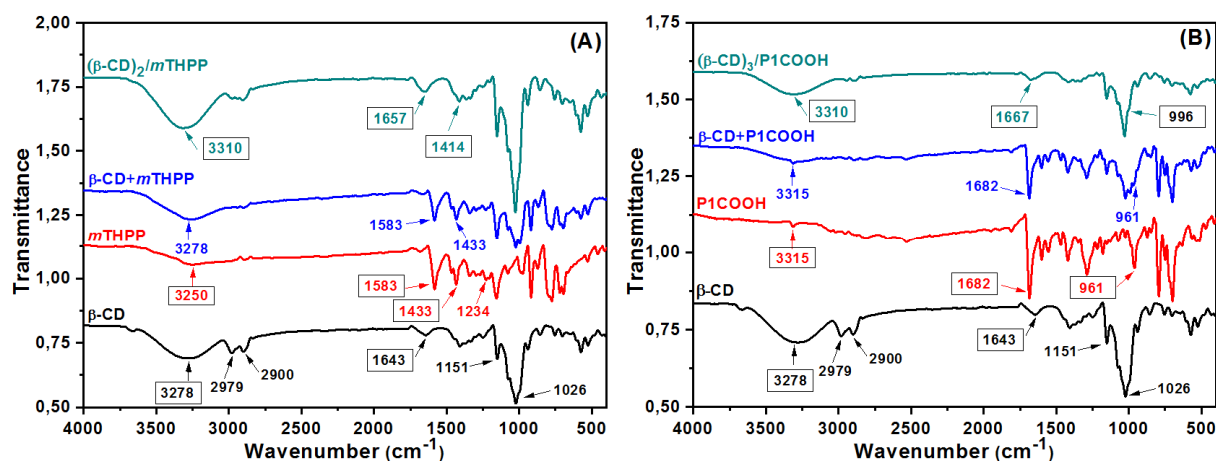
281 **Table 1.** ^1H chemical shifts (ppm) values for H1-H6 protons in $\beta\text{-CD}$ and solid $(\beta\text{-CD})_2/m\text{THPP}$ and $[(\beta\text{-CD})/$
 282 $\text{P1COOH}]_4$ inclusion complexes (300 MHz, $\text{DMSO-}d_6$, 298K).

Compound	H1	H2	H3	H4	H5	H6
$\beta\text{-CD}$	4.829	3.301	3.659	3.375	3.577	3.630
$(\beta\text{-CD})_2/m\text{THPP}$	4.831	3.304	3.678	3.377	3.599	3.637
$\Delta\delta^a$	+0.002	+0.003	+0.019	+0.002	+0.022	+0.007
$[(\beta\text{-CD})/\text{P1COOH}]_4$	4.830	3.301	3.675	3.378	3.595	3.632
$\Delta\delta^b$	+0.001	+0.000	+0.016	+0.003	+0.018	+0.002

283 ^a: $\Delta\delta = \delta ((\beta\text{-CD})_2/m\text{THPP}) - \delta (\beta\text{-CD})$; ^b: $\Delta\delta = \delta ([(\beta\text{-CD})/\text{P1COOH}]_4) - \delta (\beta\text{-CD})$.

284 FTIR is widely used to confirm the inclusion complex formation because, in general, the included part of
 285 the guest entity is shifted, disappears or its intensity is altered [36,37]. FTIR spectra of $\beta\text{-CD}$, PS, physical
 286 mixture $\beta\text{-CD}+\text{PS}$ and $(\beta\text{-CD})_n/\text{PS}$ inclusion complex for $m\text{THPP}$ and P1COOH are shown in Fig. 3. The
 287 FTIR spectrum of $\beta\text{-CD}$ consists of the broad O-H stretching band centered at 3278 cm^{-1} , the symmetric
 288 and asymmetric C-H stretching bands at 2979 and 2900 cm^{-1} , the H-O-H deformation bands at 1643 cm^{-1}
 289 due to water molecules present in $\beta\text{-CD}$, the C-O-C vibrational band at 1151 cm^{-1} , the broad C-H and C-O
 290 stretching bands around 1026 cm^{-1} . Concerning the PSs, the FTIR spectra reveal various characteristic
 291 bands relating to major functional groups contained in $m\text{THPP}$ and P1COOH . Among these functional
 292 groups, we would cite the N-H stretching bands at 3250 cm^{-1} , the C=C stretching bands of the benzene
 293 ring at 1583 and 1433 cm^{-1} , the C-O stretching band at 1234 cm^{-1} for $m\text{THPP}$, and the N-H stretching
 294 bands at 3315 cm^{-1} , the C=O stretching bands of the free acid at 1682 cm^{-1} , the C-C and C-H bending
 295 bands of the free base pyrrole around 961 cm^{-1} for P1COOH . In one hand, FTIR spectra of $\beta\text{-CD}+\text{PS}$

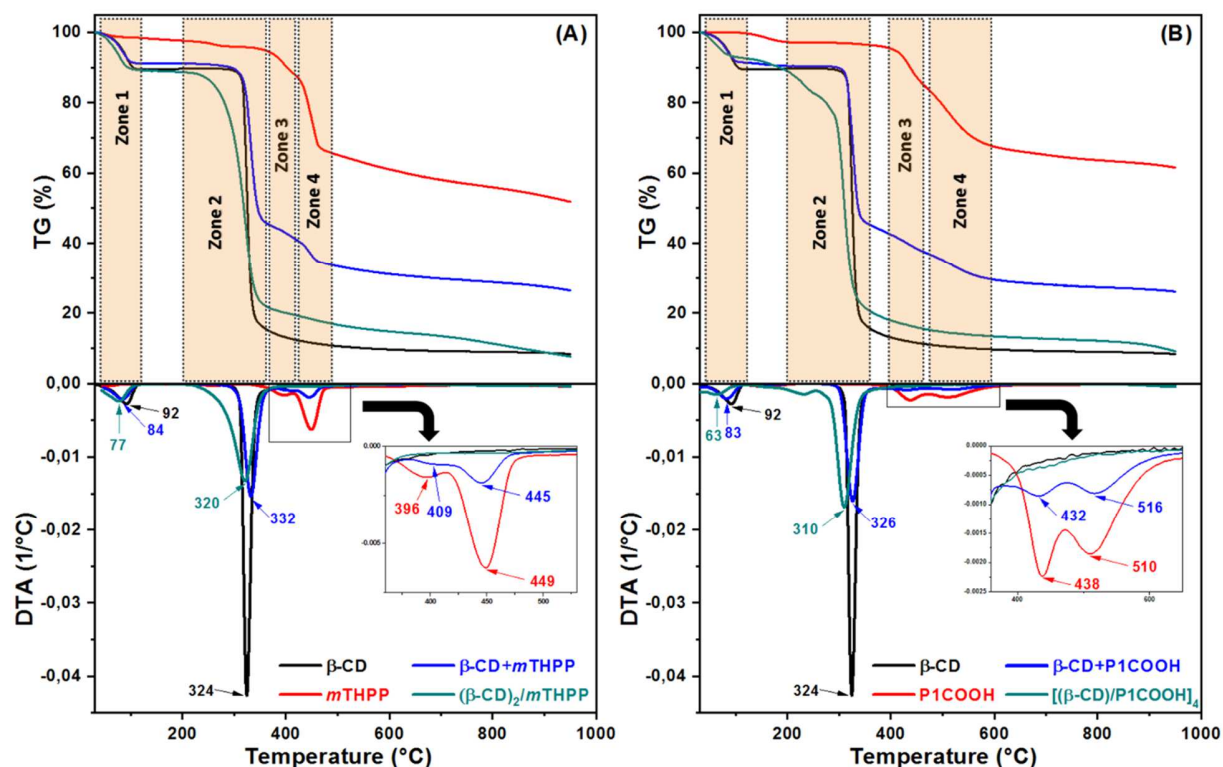
296 physical mixtures (β -CD+*m*THPP and β -CD+PICOOH) merely consist of the sum of the PS (*m*THPP or
 297 PICOOH) and β -CD spectra without apparent changes. On the other hand, the FTIR spectra of (β -
 298 CD)_n/PS inclusion complexes ((β -CD)₂/*m*THPP and [(β -CD)/PICOOH]₄) are different from those of the
 299 β -CD+PS physical mixtures and reveal important changes in several regions (*i.e.* decreased intensity,
 300 disappearance or shifting of some bands related to β -CD and PS). These changes are due to the
 301 microenvironment modifications encountered in the establishment of hydrogen bonds and van der Waals
 302 interactions between β -CD and PSs during the formation of inclusion complexes [31]. As regards the
 303 change in the C=C stretching bands of the benzene ring of *m*THPP in the (β -CD)₂/*m*THPP inclusion
 304 complex, the peak at 1433 cm⁻¹ is shifted towards 1414 cm⁻¹ and the intensity of the peak at 1583 cm⁻¹
 305 become very low until it completely disappeared. These two observations suggest that one or more of the
 306 aromatic rings of *m*THPP is inside the β -CD cavity. We may also mention the change in the C-C and C-H
 307 bending bands of the free base pyrrole of PICOOH in the [(β -CD)/PICOOH]₄ inclusion complex, the
 308 peak at 961 cm⁻¹ is shifted towards 996 cm⁻¹ indicating interactions between β -CD and the C-C and C-H
 309 groups of the free base pyrrole rings of PICOOH. To conclude we may add that the broad O-H stretching
 310 band of β -CD centered at 3278 cm⁻¹ is shifted at 3310 cm⁻¹ in both inclusion complexes signaling the
 311 establishment of hydrogen bonds between β -CD and PSs. The FTIR spectroscopy study confirms the
 312 formation of (β -CD)₂/*m*THPP and [(β -CD)/PICOOH]₄ inclusion complexes and shows that grinding
 313 method is not appropriate to form the both inclusion complexes.



314
 315 **Fig. 3.** FTIR spectra of β -CD, PS, β -CD+PS physical mixture and (β -CD)_n/PS inclusion complex for (A)
 316 *m*THPP and (B) PICOOH.

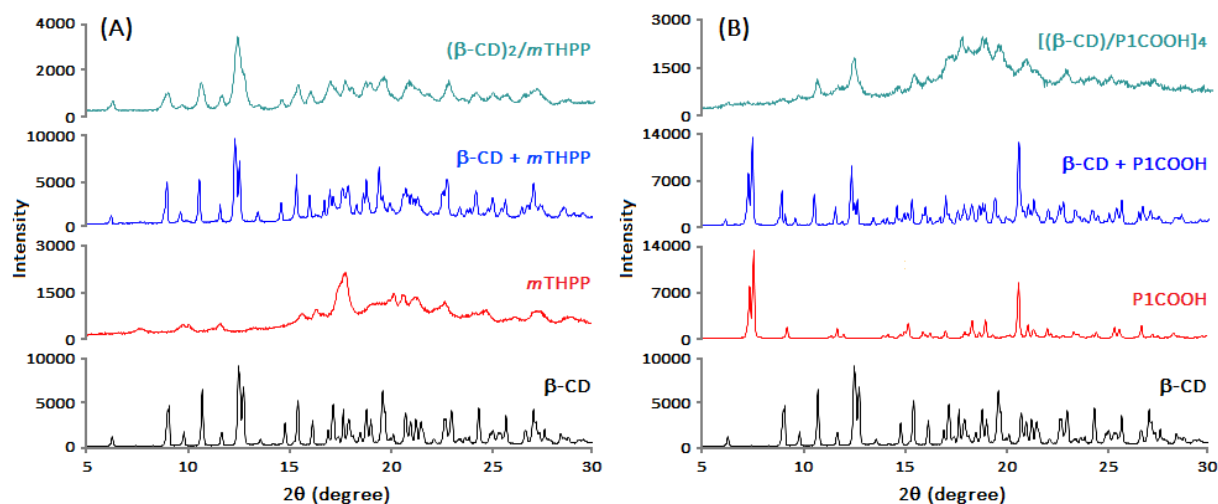
317 Another evidence of solid inclusion complexes formation is provided by thermal analyses. Among the
 318 various thermal analyses, mention may be made of complementary analyses TG and DTA. TG analysis

319 allows studying the change in the weight of the solid sample as a function of time. DTA may be
320 considered as complementary method to TG analysis of studying inclusion complexes. TG and DTA
321 curves (top and bottom figure, respectively) of β -CD, PS, physical mixture β -CD+PS and $(\beta$ -CD)_n/PS
322 inclusion complex for *m*THPP and PICOOH are shown in Fig. 4. TG and DTA curves of β -CD display
323 two zones where there is a weight loss of β -CD (Zones 1 and 2) that are associated with two endothermic
324 processes. The first zone (Zone 1) at around 92 °C with a 10 % weight loss can be attributed to a
325 dehydration process of β -CD while the second zone (Zone 2) around 324 °C with a 80 % weight loss can
326 be assigned to the fusion and decomposition of β -CD [37]. As regards the PSs (*m*THPP and PICOOH),
327 TG and DTA thermograms exhibit a continuous decomposition process beginning at around 150-200 °C
328 with a 4-5 % weight loss which could be assigned to a dehydration process of PSs, followed by a major
329 stage around 400-600 °C. This major stage can be divided in two small sub-regions (Zones 3 and 4)
330 which can be related to the decomposition process of the porphyrin rings (*i.e.* loss of chains of the
331 porphyrin rings and decomposition of the porphyrin macrocycles). The two small sub-regions are located
332 at 396 °C (8 % weight loss, Zone 3) and 409 °C (22 % weight loss, Zone 4) for *m*THPP, and at 438 °C
333 (13 % weight loss, Zone 3) and 510 °C (16 % weight loss, Zone 4) for PICOOH. For the TG and DTA
334 curves of the physical mixtures β -CD+*m*THPP and β -CD+PICOOH, the thermal behaviours are the sum
335 of the thermal behaviours of free precursors β -CD and PS (*m*THPP or PICOOH), meaning that no
336 interactions are established between β -CD and PSs. However, in the TG and DTA curves of the $(\beta$ -
337 CD)₂/*m*THPP and $[(\beta$ -CD)/PICOOH]₄ inclusion complexes, the characteristic thermal curves of PSs
338 between 400 and 600 °C disappear, which in turn suggests the establishment of interactions between β -
339 CD and PSs and thus the solid inclusion complexes formation.



340
 341 **Fig. 4.** TG (top) and DTA (bottom) curves for β -CD, PS, β -CD+PS physical mixture and $(\beta$ -CD)_n/PS
 342 inclusion complex for (A) *m*THPP and (B) P1COOH.

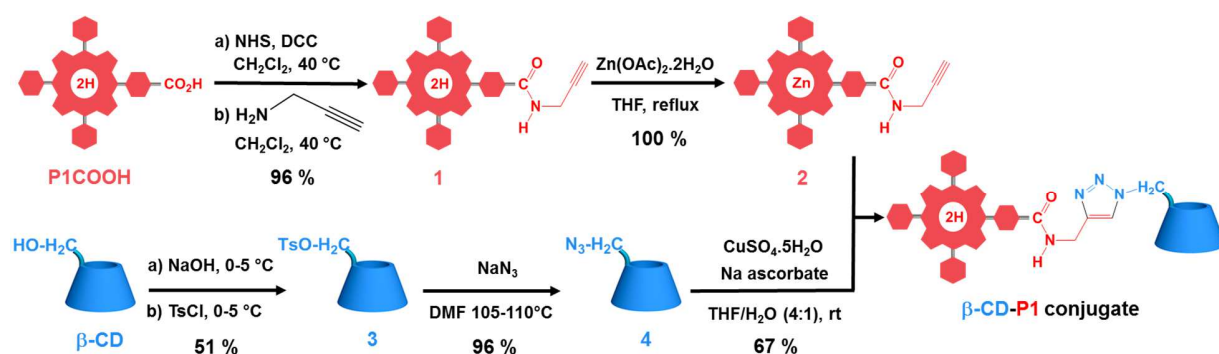
343 The latest striking evidence of the solid $(\beta$ -CD)₂/*m*THPP and $[(\beta$ -CD)/P1COOH]₄ inclusion complexes
 344 formation comes from XRD analysis. The powder XRD patterns in the 2θ range of 5° - 30° of β -CD, PS, β -
 345 CD+PS physical mixture and $(\beta$ -CD)_n/PS inclusion complex for *m*THPP and P1COOH are shown in Fig.
 346 5. The XRD diffractogram of β -CD (like P1COOH) reveals a series of sharp and intense crystalline peaks
 347 [38,39] while *m*THPP is amorphous with broad diffraction peaks distributed in a wide 2θ range.
 348 Compared with the XRD patterns of the physical mixtures containing all peaks of β -CD and PSs with a
 349 slight change of intensity and position, the sharp crystalline peaks of β -CD disappear in the XRD patterns
 350 of the solid inclusion complexes, confirming the spatial entrapment of PSs inside de cavity of β -CD and
 351 thus the inclusion complexes formation.



352
 353 **Fig. 5.** Powder XRD patterns of β -CD, PS, β -CD+PS physical mixture and $(\beta\text{-CD})_n$ /PS inclusion complex
 354 for (A) *m*THPP and (B) P1COOH.

355 **3.3. Synthesis of β -CD)-PS conjugate**

356 In parallel to the preparation of the solid $(\beta\text{-CD})_n$ /PS inclusion complexes with non-covalent bonding
 357 between β -CD and PSs, the synthesis of covalent conjugate β -CD-P1 was also undertaken by combining
 358 P1COOH with β -CD *via* a triazole covalent link. Only P1COOH as PS was used with the aim of
 359 providing exclusively the mono-functionalization of the PS with β -CD. The triazole covalent link was
 360 obtained by CuAAC click chemistry. To achieve this goal, propargyl-modified ZnP1COOH **2** and azide-
 361 modified β -CD **4** were prepared (Fig. 6).



362
 363 **Fig. 6.** Synthetic route for β -CD-P1 conjugate.

364 Propargyl-modified ZnP1COOH **2** was prepared in two steps with 96 % overall yield according to the
 365 protocol previously described by our team (Fig. 6) [22]. First, the carboxylic function of P1COOH was

366 activated *in situ* as NHS ester using dicyclohexylcarbodiimide (DCC) and *N*-hydroxysuccinimide (NHS),
367 then coupled with propargylamine to afford the propargyl-modified PICOOH **1** in 96 % yield. Secondly,
368 the porphyrin ring of **1** was metalated with Zn(OAc)₂ to provide the desired propargyl-modified
369 ZnPICOOH **2** in quantitative yield. The metalation step was essential to avoid copper metalation of the
370 porphyrin ring during the subsequent CuAAC reaction.

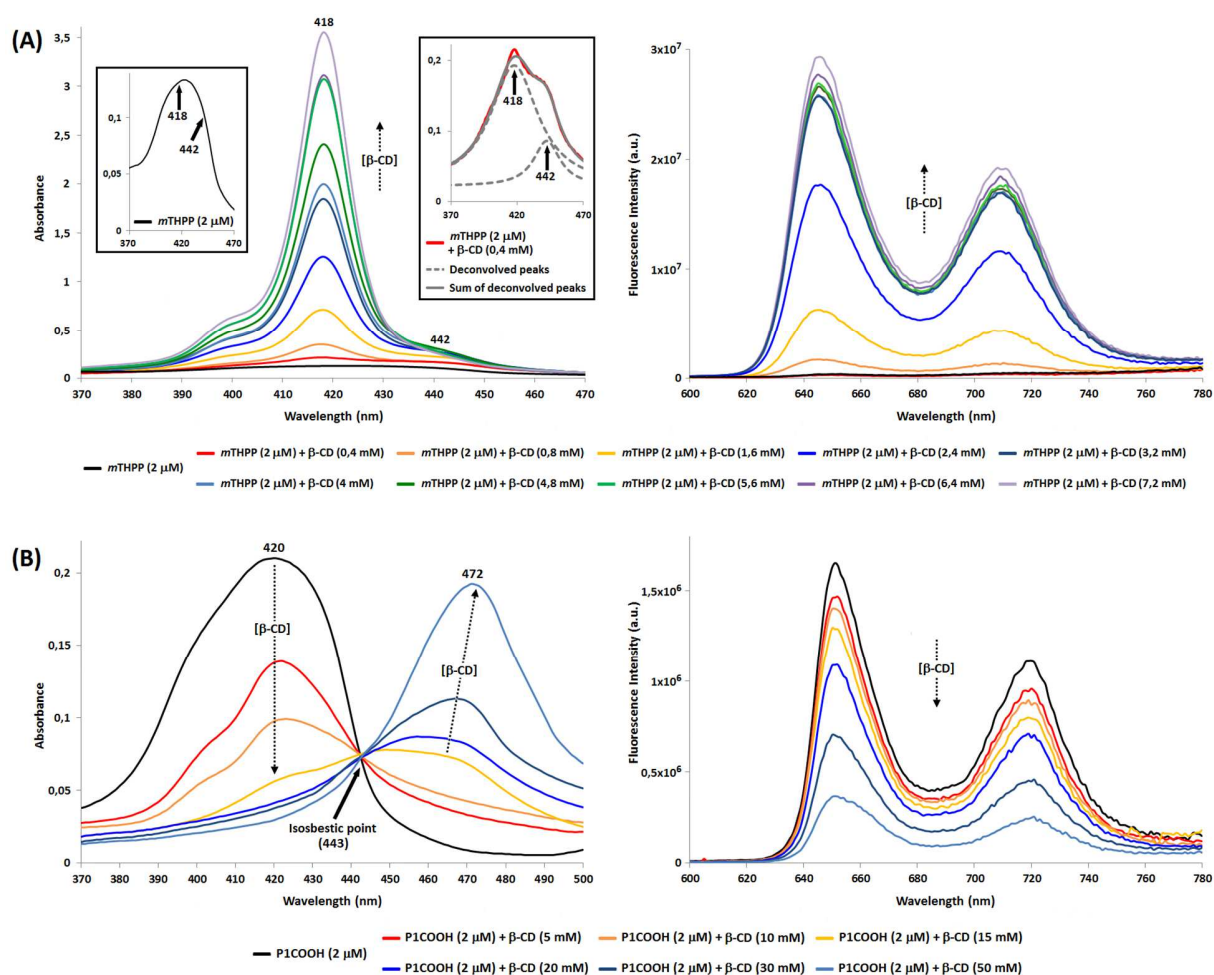
371 Azide-modified β-CD **4** was prepared in two-step procedure in 49 % overall yield (Fig. 6). First, the
372 secondary hydroxyl groups of β-CD were tosylated using tosyl chloride to provide β-CD-OTs **3** in 51 %
373 yield according to a previous protocol described by our team [23] with slight modifications. Second, tosyl
374 groups of β-CD-OTs **3** were subjected to a nucleophilic substitution with sodium azide to provide azide-
375 modified β-CD **4** in 96 % yield according to a previous protocol described in the literature [24].

376 Finally, the synthesis of the conjugate β-CD-P1 was obtained using CuAAC click chemistry between **2**
377 and **4** *via* triazole covalent link formation in 67 % yield (Fig. 6). It is noted that the demetalation of the
378 porphyrin ring occurred during the purification step.

379 3.4. Disaggregation study in aqueous medium

380 The disaggregation effect of β-CD on PS (*m*THPP or PICOOH) in aqueous medium is investigated using
381 a fixed PS concentration of 2 μM and a varied β-CD concentration from 0 to 50 mM. The UV-vis
382 absorption and fluorescence emission spectra of PS with different concentrations of β-CD are shown in
383 Fig. 7. UV-vis spectrum of *m*THPP in milli-Q water displays the presence of very broad Soret band which
384 is due to the combination of aggregates and monomers of *m*THPP without the possibility to assign a
385 specific wavelength for each species (Fig. 7A). Addition of β-CD (from 0 to 7.2 mM) is found to make
386 the Soret band more narrow leading us to deduce by deconvolution that the very broad Soret band
387 consists of two superimposed bands located at 418 nm and 442 nm. It is generally accepted that a red-
388 shift in the UV-vis absorption spectra relatively to that of the monomer is proof of J-aggregate and also
389 aggregation leads to the fluorescence quenching [40]. As shown in Fig. 7A, the absorbance intensity of
390 the peak at 418 nm and the fluorescence intensity increase significantly with the increasing concentration
391 of β-CD, which allows assigning the peaks at 418 nm and 442 nm to *m*THPP monomers and J-aggregates,
392 respectively. Furthermore, it is worth noting that generally, the formation of an inclusion complex with
393 cyclodextrins does not affect the UV-vis spectrum of small molecules [41]. Based on this information, we
394 can also assign the peak at 418 nm to the monomeric inclusion complex between *m*THPP and β-CD. All
395 these results highlight the β-CD's ability to reduce the formation of *m*THPP aggregates through the
396 formation of monomeric inclusion complex. The UV-vis spectrum of PICOOH in milli-Q water shows

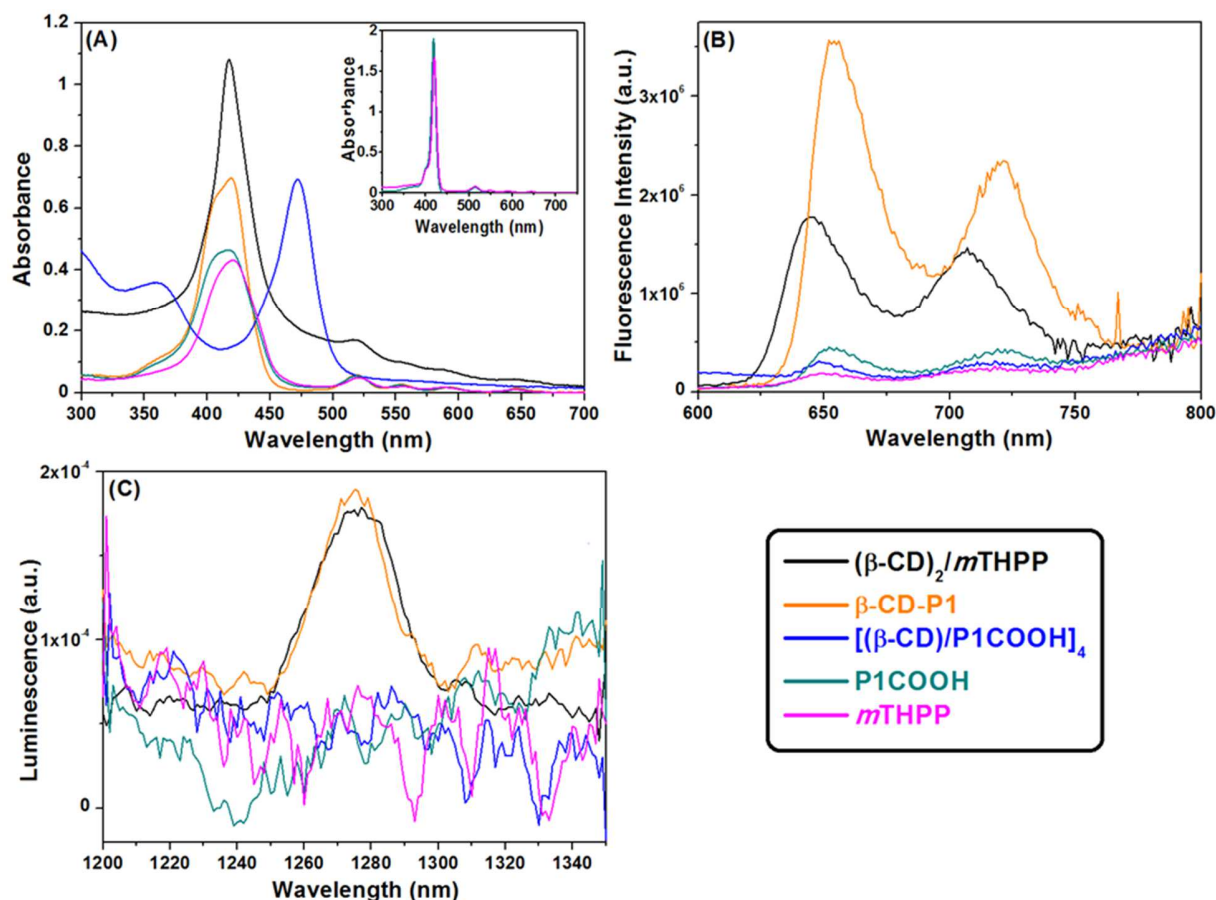
397 also a similar broad Soret band to *m*THPP (Fig. 7B) and the same results can be expected. Surprisingly, a
 398 noticeable decrease of the P1COOH monomers peak at around 420 nm is observed with the addition of β -
 399 CD (from 0 to 50 mM), accompanied by the appearance of an isosbestic point in the absorption spectra at
 400 443 nm and an increasing absorption at 472 ppm (Fig. 7B). Furthermore, the fluorescence intensity
 401 decreases notably with the increasing concentration of β -CD indicating that a phenomenon of aggregation
 402 still occurs. The presence of the isosbestic point and the red shifted peak at 472 nm confirm the formation
 403 of the inclusion complex and seem to indicate the establishment of an equilibrium between monomeric
 404 inclusion complex (420 nm) and unknown J-aggregates (472 nm). Based on the results obtained from
 405 Job's and Benesi-Hildebrand plots (see Section 3.1.), the peak at 472 nm can be assigned to J-tetramer
 406 aggregates of the 1:1 inclusion complex.



407
 408 **Fig. 7.** UV-vis and fluorescence spectra of (A) *m*THPP (2 μ M) and (B) P1COOH (2 μ M) containing
 409 various concentration of β -CD in milli-Q water.

410 3.5. Binding type effect on PSs disaggregation in aqueous medium

411 The binding type effect of β -CD on the disaggregation of PSs (*m*THPP or P1COOH) in aqueous medium
412 is investigated by comparing the photophysical properties of the free PSs and β -CD/PS systems in D₂O.
413 The UV-vis absorption, fluorescence emission and ¹O₂ luminescence spectra of the three β -CD/PS
414 systems in D₂O are given in Fig. 8. The UV-vis spectra of the free *m*THPP and P1COOH in DMSO are
415 characterized by a narrow Soret band (monomeric species, disaggregated state) at 421 nm and 419 nm,
416 respectively, and four Q bands between 510 and 650 nm for each one (insert in the top right of the Fig.
417 8A). Coherence-consistent changes are observed on the UV-vis spectra of the two PSs when D₂O is used
418 as solvent. The appearance of very broad Soret bands in UV-vis spectra of the free PSs in D₂O (Fig. 8A,
419 pink and green curves), accompanied by their fluorescence emission and ¹O₂ luminescence quenching
420 (Figs. 8B and 8C, pink and green curves), reveal the propensity of these PSs to self-aggregate in D₂O
421 [42]. As already observed in the disaggregation study with *m*THPP (see Section 3.4.), the UV-vis
422 spectrum of (β -CD)₂/*m*THPP inclusion complex shows an increase in absorbance intensity and sharpening
423 of the Soret band at 418 nm compared to free *m*THPP (Fig. 8A, pink and black curves), indicating a
424 significantly lower degree of aggregation and thus the formation of the monomeric inclusion complex in
425 D₂O. The formation of the (β -CD)₂/*m*THPP inclusion complex in monomeric form in D₂O is also
426 evidenced by an increase of the fluorescence emission and ¹O₂ luminescence (Figs. 8B and 8C, black
427 curves) with fluorescence and ¹O₂ quantum yields of 1 % and 16 %, respectively. Compared to P1COOH
428 alone, the UV-vis spectrum of [(β -CD)/P1COOH]₄ inclusion complex in D₂O shows a slight broadening
429 and remarkable red shift of the Soret band from 420 nm to 472 ppm (Fig. 8A, green and blue curves), as
430 already observed in the disaggregation study with P1COOH (see Section 3.4.), revealing the existence of
431 a phenomenon of aggregation and the formation of J-tetramer aggregates of the 1:1 inclusion complex.
432 The high J-type self-aggregation of [(β -CD)/P1COOH]₄ inclusion complex in D₂O is also supported by
433 fluorescence emission and ¹O₂ luminescence quenching (Figs. 8B and 8C, blue curves). Finally, in
434 contrast to a non-covalent link between P1COOH and β -CD in [(β -CD)/P1COOH]₄ inclusion complex,
435 the use of a covalent bond in β -CD-P1 conjugate shows similar observations to those made for the (β -
436 CD)₂/*m*THPP inclusion complex in D₂O, *i.e.* increased intensity and sharpening of the Soret band at
437 around 420 nm compared to P1COOH (Fig. 8A, green and orange curves) with an increase of the
438 fluorescence emission and ¹O₂ luminescence yielding fluorescence and ¹O₂ quantum yields of 2 % and 16
439 %, respectively (Figs. 8B and 8C, orange curves). These observations demonstrate that the use of a
440 covalent link between P1COOH and β -CD allows the formation of the monomeric species (non-
441 aggregated β -CD-P1 conjugate) in D₂O.



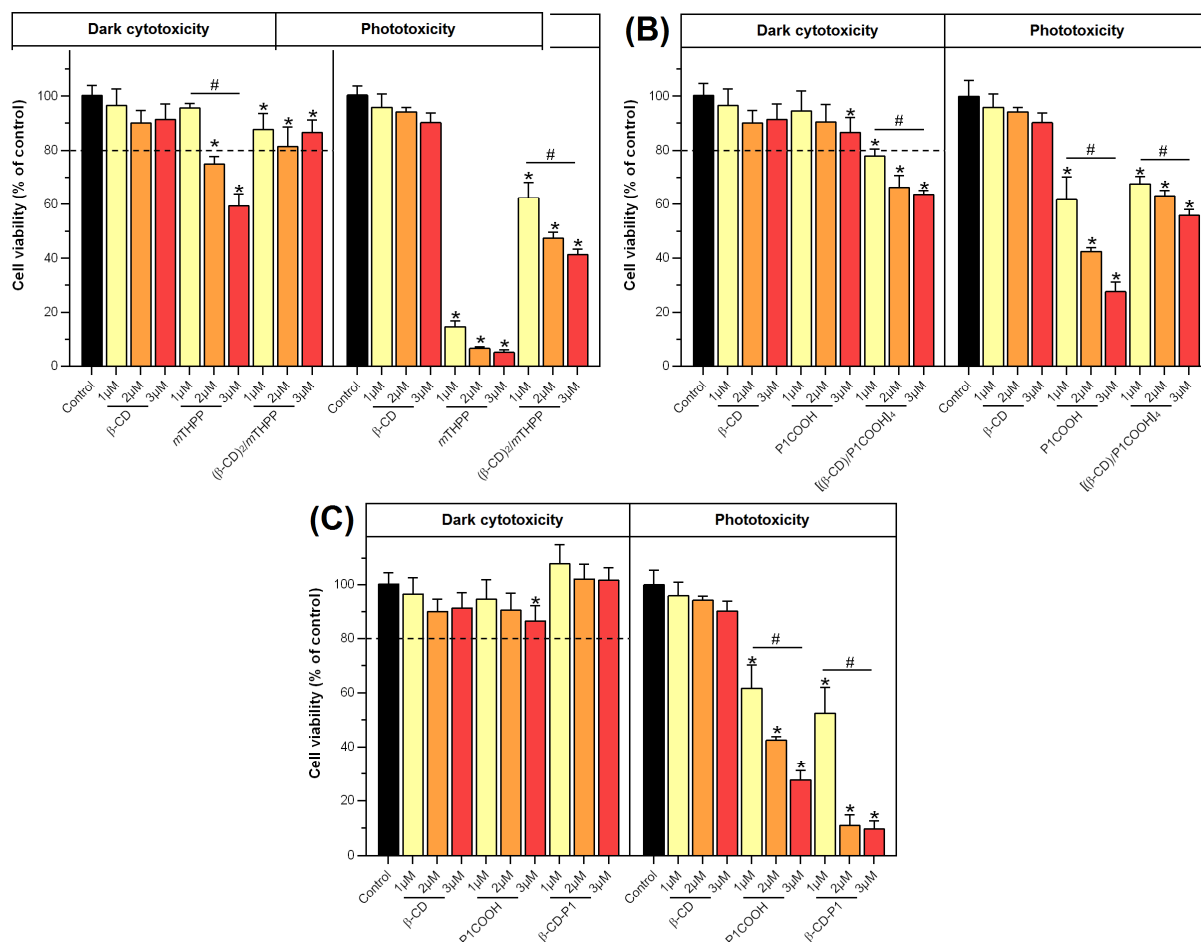
442
 443 **Fig. 8.** Photophysical properties of *m*THPP, P1COOH and the three β -CD/PS systems ($\lambda_{\text{exc.}} = 419$ nm).
 444 (A) Absorption spectra at a single concentration of DMSO and D₂O ([PS] = 4 μ M) (the insert in the top
 445 right corner depicts the absorption spectra in DMSO), (B) fluorescence emission spectra, and (C) ¹O₂
 446 luminescence at a single concentration of D₂O (equal Soret bands at 0.2 ± 0.05 by dilution).

447 All these results indicate that both binding type between β -CD and PS can help to improve disaggregation
 448 of PSs in aqueous medium (*i.e.* (β -CD)₂/*m*THPP inclusion complex and β -CD-P1 conjugate in monomeric
 449 forms in D₂O). In the case of non-covalent link, it should be noted that the improvement in disaggregation
 450 can be hampered by self-aggregation of the inclusion complex itself (*i.e.* [(β -CD)/P1COOH]₄ inclusion
 451 complex).

452 3.6. Binding type effect on *in vitro* PDT efficacy of PSs

453 The binding type effect of β -CD on the *in vitro* PDT efficacy of PSs is investigated by comparing the *in*
 454 *vitro* dark cytotoxicity and phototoxicity of the free PSs and β -CD/PS systems at different PS
 455 concentrations (1, 2 and 3 μ M) using human glioblastoma U87 cancer cells. After 24 h of incubation at 37

456 °C in the dark or after PDT treatment (652 nm, 10 J/cm², 36 min), cell viability is determined by the MTT
457 assay as previously described [27]. The results of *in vitro* dark cytotoxicity and phototoxicity assays are
458 presented in Fig. 9. It is worth noting that β-CD alone displays no dark cytotoxicity and phototoxicity on
459 U87 cells within the concentration range used (from 1 to 3 μM). The dark cytotoxicity of free PSs on U87
460 cells (Figs. 9A and 9B) reveals a higher dark cytotoxic effect for *m*THPP than P1COOH suggesting that
461 U87 cells are more sensitive to *m*THPP. As regards the comparison between *m*THPP and solid (β-
462 CD)₂/*m*THPP inclusion complex, Fig. 9A indicates that inclusion complex reduces the dark cytotoxicity
463 of *m*THPP, which could be explained by the fact that the inclusion of PS into β-CD host cavity limits
464 direct contact between cells and PS, helping to reduce the dark cytotoxicity of *m*THPP. The opposite
465 result obtained for P1COOH and solid [(β-CD)/P1COOH]₄ inclusion complex (*i.e.* inclusion complex
466 more dark cytotoxic) could be explained by the high J-type self-aggregation of the inclusion complex in
467 tetrameric form (see Sections 3.4. and 3.5.). With regard to the higher phototoxicity of free PSs relative to
468 their inclusion complexes (Figs. 9A and 9B), a possible explanation is that the entrapment of the PS into
469 the host cavity of β-CD reduces direct contact between cells and PS or at least reduces the time required
470 for this interaction to occur, as recently suggested by T. A. Reis et al. [43]. Finally, comparative dark
471 cytotoxicity and phototoxicity data for free P1COOH and β-CD-P1 conjugate (Fig. 9C) show that β-CD-
472 P1 conjugate has the best *in vitro* PDT efficacy against glioblastoma U87 cells among the three β-CD/PS
473 systems studied. The covalent conjugation of P1COOH to β-CD through a triazole link avoids
474 aggregation compared to the solid [(β-CD)/P1COOH]₄ inclusion complex (see Sections 3.4. and 3.5.),
475 leading to no dark cytotoxic effect and better PDT efficiency of β-CD-P1 conjugate on U87 cells (cell
476 viability of 9 % at 3 μM). The *in vitro* PDT effectiveness of β-CD-P1 conjugate (from 1 to 20 μM) is also
477 evidenced on human glioblastoma U251 cells resulting in no dark cytotoxicity and high phototoxicity
478 (cell viability of 3 % at 3 μM, see Supporting Information, Fig. S6).



479
 480 **Fig. 9.** Cell viability of U87 cells treated with (A) $(\beta\text{-CD})_2/m\text{THPP}$, (B) $[(\beta\text{-CD})/P\text{ICOOH}]_4$ and (C) $\beta\text{-CD-P1}$
 481 at PS concentration of 1-3 μM incubated into the dark (left, dark cytotoxicity) or after irradiation
 482 using a diode laser at a wavelength of 652 nm at a fluence of 10 J/cm^2 during 36 min (right,
 483 phototoxicity). Results were expressed as percentage of values obtained from untreated cells and given by
 484 mean \pm SD, $n = 3$, $p \leq 0.05$. * Vs. control cells. # Vs. same compound at smaller concentration.

485 **4. Conclusions**

486 Three new $\beta\text{-CD}/\text{PS}$ systems (*i.e.* solid $(\beta\text{-CD})_2/m\text{THPP}$ and $[(\beta\text{-CD})/P\text{ICOOH}]_4$ inclusion complexes
 487 and $\beta\text{-CD-P1}$ conjugate) are successfully synthesized *via* two different binding types (*i.e.* non-covalent
 488 and covalent) between $\beta\text{-CD}$ and hydrophobic PS. The binding type effect and effectiveness on the
 489 disaggregation in aqueous medium and *in vitro* PDT efficacy against glioblastoma cancer cells of PSs are
 490 investigated.

492 The findings indicate that both binding type between β -CD and PS lead to an improvement of PSs
493 disaggregation in aqueous medium but for the non-covalent binding type, this improvement could be
494 hampered by self-aggregation of the inclusion complex itself. In addition, *in vitro* PDT activity against
495 human glioblastoma cells reveals a higher *in vitro* PDT efficacy when the covalent binding type is used.
496 As answer to our above hypothesis, the disaggregation in aqueous medium and *in vitro* anticancer PDT
497 activity of hydrophobic PSs can be improved by their binding to β -CD and the covalent binding type is
498 the most effective approach.

499 **Authors contributions**

500 This work was designed and supervised by S.A. The synthesis and characterization (FTIR, TG, DTA,
501 powder XRD, NMR...) of the three β -CD/PS systems were conducted by A.B.M with the advice and
502 assistance of L.C. The photophysical analyses (UV-vis, florescence and $^1\text{O}_2$ luminescence) were
503 supervised by P.A. and C.F. *In vitro* studies were performed by Z.Y. and V.J.H. The draft manuscript was
504 co-written by S.A., A.B.M. and R.V. All authors have given approval to the final version of the
505 manuscript.

506 **Declaration of Competing Interest**

507 The authors declare no competing financial interest.

508 **Acknowledgements**

509 A.B.M. is supported by the Algerian Ministry of Higher Education and Scientific Research scholarship
510 (No: 115/PNE: 2016/2017). The authors acknowledge Mathilde Achard for performing Mass experiments
511 and Olivier Favre for running NMR experiments.

512 **References**

513 [1] Ackroyd, R., Kelty, C., Brown, N., and Reed, M. (2001). The history of photodetection and
514 photodynamic therapy. *Photochemistry and Photobiology*, 74, 656–669.
515 [https://doi.org/10.1562/0031-8655\(2001\)0740656THOPAP2.0.CO2](https://doi.org/10.1562/0031-8655(2001)0740656THOPAP2.0.CO2).

- 516 [2] Josefsen, L. B., and Boyle, R. W. (2012). Unique diagnostic and therapeutic roles of porphyrins
517 and phthalocyanines in photodynamic therapy, imaging and theranostics. *Theranostics*, 2, 916–
518 966. <https://doi.org/10.7150/thno.4571>.
- 519 [3] Staggers, N., McCasky, T., Brazelton, N., and Kennedy, R. (2008). Nanotechnology: The coming
520 revolution and its implications for consumers, clinicians, and informatics. *Nursing Outlook*, 56,
521 268–274. <https://doi.org/10.1016/j.outlook.2008.06.004>.
- 522 [4] Marchal, S., El Hor, A., Millard, M., Gillon, V., and Bezdetnaya, L. (2015). Anticancer drug
523 delivery: An update on clinically applied nanotherapeutics. *Drugs*, 75, 1601–1611.
524 <https://doi.org/10.1007/s40265-015-0453-3>.
- 525 [5] Reshetov, V., Lassalle, H. P., Francois, A., Dumas, D., Hupont, S., Gräfe, S., Filipe, V., Jiskoot,
526 W., Guillemin, F., Zorin, V., and Bezdetnaya, L. (2013). Photodynamic therapy with
527 conventional and PEGylated liposomal formulations of mTHPC (temoporfin): Comparison of
528 treatment efficacy and distribution characteristics *in vivo*. *International Journal of Nanomedicine*,
529 8, 3817–3831. <https://doi.org/10.2147/IJN.S51002>.
- 530 [6] Ogawara, K.-i., Shiraishi, T., Araki, T., Watanabe, T.-i., Ono, T., and Higaki, K. (2016). Efficient
531 anti-tumor effect of photodynamic treatment with polymeric nanoparticles composed of
532 polyethylene glycol and polylactic acid block copolymer encapsulating hydrophobic porphyrin
533 derivative. *European Journal of Pharmaceutical Sciences*, 82, 154–160.
534 <https://doi.org/10.1016/j.ejps.2015.11.016>.
- 535 [7] Kryjewski, M., Goslinski, T., and Mielcarek, J. (2015). Functionality stored in the structures of
536 cyclodextrin–porphyrinoid systems. *Coordination Chemistry Reviews*, 300, 101–120.
537 <https://doi.org/10.1016/j.ccr.2015.04.009>.
- 538 [8] Mazzaglia, A. (2011). Photodynamic tumor therapy with cyclodextrin nanoassemblies.
539 Cyclodextrins in Pharmaceutics, Cosmetics, and Biomedicine (Bilensoy, E., Ed.) pp 343–361,
540 Chapter 18, John Wiley & Sons, Inc., Hoboken. <https://doi.org/10.1002/9780470926819.ch18>.
- 541 [9] Cheirsilp, B., and Rakmai, J. (2016). Inclusion complex formation of cyclodextrin with its guest
542 and their applications. *Biology, Engineering and Medicine*, 2, 1–6.
543 <https://doi.org/10.15761/BEM.1000108>.
- 544 [10] Das, S. K., Rajabalaya, R., David, S., Gani, N., Khanam, J., and Nanda, A. (2013). Cyclodextrins-
545 The molecular container. *Research Journal of Pharmaceutical, Biological and Chemical
546 Sciences*, 4, 1694–172. ISSN: 0975-8585
- 547 [11] Dodziuk, H. (2006). Molecules with holes-cyclodextrins. *Cyclodextrins and Their Complexes:
548 Chemistry, Analytical Methods, Applications* (Dodziuk, H., Ed.) pp. 1–30, Chapter 1, Wiley-
549 VCH Verlag GmbH & Co. KGaA, Weinheim. <https://doi.org/10.1002/3527608982.ch1>.

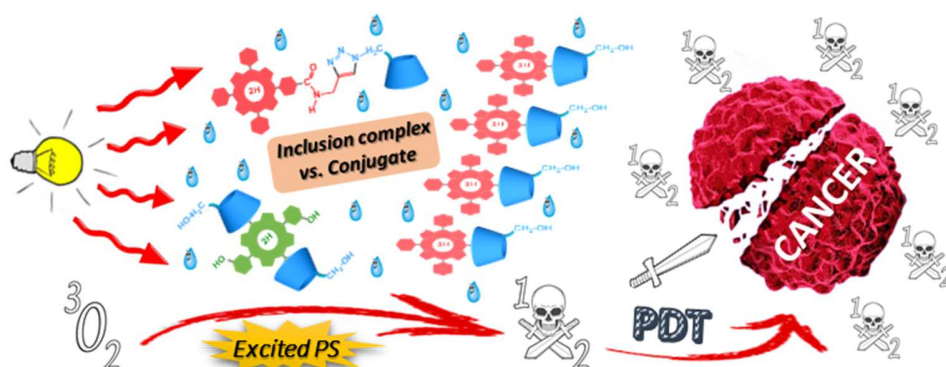
- 550 [12] Patil, J. S., Kadam, D. V., Marapur, S. C., and Kamalapur, M. V. (2010). Inclusion complex
551 system; a novel technique to improve the solubility and bioavailability of poorly soluble drugs: A
552 review. *International Journal of Pharmaceutical Sciences Review and Research*, 2, 29–34.
- 553 [13] Zarzycki, P. K., Fenert, B., and Głód, B. K. (2016). Cyclodextrins-based nanocomplexes for
554 encapsulation of bioactive compounds in food, cosmetics, and pharmaceutical products:
555 Principles of supramolecular complexes formation, their influence on the antioxidative properties
556 of target chemicals, and recent advances in selected industrial applications. *Encapsulations:
557 Nanotechnology in the Agri-Food Industry Volume 2* (Grumezescu, A. M., Ed.) pp. 717–767,
558 Chapter 17, Academic Press, Cambridge. <https://doi.org/10.1016/B978-0-12-804307-3.00017-X>.
- 559 [14] Iacovino, R., Caso, J. V., Donato, C. D., Malgieri, G., Palmieri, M., Russo, L., and Isernia, C.
560 (2017). Cyclodextrins as complexing agents: Preparation and applications. *Current Organic
561 Chemistry*, 21, 162–176. <https://doi.org/10.2174/1385272820666160909111842>.
- 562 [15] Conte, C., Scala, A., Siracusano, G., Sortino, G., Pennisi, R., Piperno, A., Miro, A., Ungaro, F.,
563 Sciortino, M. T., Quaglia, F. et al. (2016). Nanoassemblies based on non-ionic amphiphilic
564 cyclodextrin hosting Zn(II)-phthalocyanine and docetaxel: Design, physicochemical properties
565 and intracellular effects. *Colloids and Surfaces B: Biointerfaces*, 146, 590–597.
566 <https://doi.org/10.1016/j.colsurfb.2016.06.047>.
- 567 [16] Kirejev, V., Goncalves, A. R., Aggelidou, C., Manet, I., Martensson, J., Yannakopoulou, K., and
568 Ericson, M. B. (2014). Photophysics and *ex vivo* biodistribution of beta-cyclodextrin-meso-
569 tetra(m-hydroxyphenyl)porphyrin conjugate for biomedical applications. *Photochemical &
570 Photobiological Sciences*, 13, 1185–1191. <https://doi.org/10.1039/C4PP00088A>.
- 571 [17] Mazzaglia, A., Sciortino, M. T., Kandoth, N., and Sortino, S. (2012). Cyclodextrin-based
572 nanoconstructs for photoactivated therapies. *Journal of Drug Delivery Science and Technology*,
573 22, 235–242. [https://doi.org/10.1016/S1773-2247\(12\)50034-1](https://doi.org/10.1016/S1773-2247(12)50034-1).
- 574 [18] Yankovsky, I., Bastien, E., Yakavets, I., Khludeyev, I., Lassalle, H. P., Gräfe, S., Bezdetnaya, L.,
575 and Zorin, V. (2016). Inclusion complexation with beta-cyclodextrin derivatives alters
576 photodynamic activity and biodistribution of meta-tetra(hydroxyphenyl)chlorin. *European
577 Journal of Pharmaceutical Sciences*, 91, 172–182. <https://doi.org/10.1016/j.ejps.2016.06.012>.
- 578 [19] Ben Mihoub, A., Larue, L., Moussaron, A., Youssef, Z., Colombeau, L., Baros, F., Frochet, C.,
579 Vanderesse, R., and Acherar, S. (2018). Use of cyclodextrins in anticancer photodynamic therapy
580 treatment. *Molecules*, 23, 1936. <https://doi.org/10.3390/molecules23081936>.
- 581 [20] Job, P. (1928). Formation and stability of inorganic complexes in solution. *Annali di Chimica
582 Applicata*, 9, 113–203.

- 583 [21] Catena, G. C., and Bright, F. V. (1989). Thermodynamic study on the effects of beta-cyclodextrin
584 inclusion with anilinonaphthalenesulfonates. *Analytical Chemistry*, 61, 905–909.
585 <https://doi.org/10.1021/ac00183a024>.
- 586 [22] Mohd Gazzali, A., Colombeau, L., Arnoux, P., Wahab, H. A., Frochot, C., Vanderesse, R., and
587 Acherar, S. (2017). Synthesis of mono-, di- and triporphyrin building blocks by click chemistry
588 for photodynamic therapy application. *Tetrahedron*, 73, 532–541.
589 <https://doi.org/10.1016/j.tet.2016.12.037>.
- 590 [23] Ben Mihoub, A., Saidat, B., Bal, Y., Frochot, C., Vanderesse, R., and Acherar, S. (2018).
591 Development of new ionic gelation strategy: Towards the preparation of new monodisperse and
592 stable hyaluronic acid/b-cyclodextrin-grafted chitosan nanoparticles as drug delivery carriers for
593 doxorubicin. *Frontiers of Materials Science*, 12, 83–94. [https://doi.org/10.1007/s11706-018-](https://doi.org/10.1007/s11706-018-0407-2)
594 [0407-2](https://doi.org/10.1007/s11706-018-0407-2).
- 595 [24] Xu, M., Wu, S., Zeng, F., and Yu, C. (2010). Cyclodextrin supramolecular complex as a water-
596 soluble ratiometric sensor for ferric ion sensing. *Langmuir*, 26, 4529–4534.
597 <https://doi.org/10.1021/la9033244>.
- 598 [25] Seybold, P. G., and Gouterman, M. (1969). Porphyrins: XIII: Fluorescence spectra and quantum
599 yields. *Journal of Molecular Spectroscopy*, 31, 1–13. [https://doi.org/10.1016/0022-](https://doi.org/10.1016/0022-2852(69)90335-X)
600 [2852\(69\)90335-X](https://doi.org/10.1016/0022-2852(69)90335-X).
- 601 [26] Wilkinson, F., Helman, W. P., and Ross, A. B. (1993). Quantum yields for the photosensitized
602 formation of the lowest electronically excited singlet oxygen state of molecular oxygen in
603 solution. *Journal of Physical and Chemical Reference Data*, 22, 113–262.
604 <https://doi.org/10.1063/1.555934>.
- 605 [27] Pramual, S., Lirdprapamongkol, K., Svasti, J., Bergkvist, M., Jouan-Hureau, V., Arnoux, P.,
606 Frochot, C., Barberi-Heyob, M., and Niamsiri, N. (2017). Polymer-lipid-PEG hybrid
607 nanoparticles as photosensitizer carrier for photodynamic therapy. *Journal of Photochemistry and*
608 *Photobiology B: Biology B*, 173, 12–22. <https://doi.org/10.1016/j.jphotobiol.2017.05.028>.
- 609 [28] Bonnett, R. (2000). Photobleaching. *Chemical Aspects of Photodynamic Therapy Volume 1*
610 (Phillips, D., O'Brien, P., and Roberts, S., Eds.) pp 237–256, Chapter 12, Gordon and Breach
611 Science Publishers, London. <https://doi.org/10.1201/9781482296952>.
- 612 [29] Hunter, C. A., and Sanders, M. K. J. (1990). The nature of π - π interactions. *Journal of the*
613 *American Chemical Society*, 112, 5525–5534. <https://doi.org/10.1021/ja00170a016>.
- 614 [30] Siggel, U., Bindig, U., Endisch, C., Komatsu, T., Tsuchida, E., Voigt, E., and Fuhrhop, J. H.
615 (1996). Photophysical and photochemical properties of porphyrin aggregates. *Berichte der*

- 616 *Bunsengesellschaft für Physikalische Chemie*, 100, 2070–2075.
617 <https://doi.org/10.1002/bbpc.19961001225>.
- 618 [31] Aggelidou, C., Theodossiou, T. A., and Yannakopoulou, K. (2013). Protoporphyrin IX- β -
619 cyclodextrin bimodal conjugate: Nanosized drug transporter and potent phototoxin.
620 *Photochemistry and Photobiology*, 89, 1011–1019. <https://doi.org/10.1111/php.12127>.
- 621 [32] Tau, P., Ogunsipe, A. O., Maree, S., Maree, M. D., and Nyokong, T. (2003). Influence of
622 cyclodextrins on the fluorescence, photostability and singlet oxygen quantum yields of zinc
623 phthalocyanine and naphthalocyanine complexes. *Journal of Porphyrins and Phthalocyanines*, 7,
624 439–446. <https://doi.org/10.1142/S1088424603000562>.
- 625 [33] Schneider, H.-J., Hacket, F., Rüdiger, V., and Ikeda, H. (1998). NMR studies of cyclodextrins and
626 cyclodextrin complexes. *Chemical Reviews*, 98, 1755–1786. <https://doi.org/10.1021/cr970019t>.
- 627 [34] Answer, M. K., Jamil, S., Ansari, M. J., Al-Shdefat, R., Ali, B. E., Ganaie, M. A., Abdel-Kader,
628 M. S., and Shakeel, F. (2014). Water soluble binary and ternary complexes of diosmin with β -
629 cyclodextrin: Spectroscopic characterization, release studies and anti-oxidant activity. *Journal of*
630 *Molecular Liquids*, 199, 35–41. <https://doi.org/10.1016/j.molliq.2014.08.012>.
- 631 [35] Gao, S., Liu, Y., Jiang, J., Ji, Q., Zhao, L., Li, C., and Ye, F. (2019). Physicochemical properties
632 and fungicidal activity of inclusion complexes of fungicide chlorothalonil with β -cyclodextrin and
633 hydroxypropyl- β -cyclodextrin. *Journal of Molecular Liquids*, 293, 111513.
634 <https://doi.org/10.1016/j.molliq.2019.111513>.
- 635 [36] Ahmed, S. M., Naggi, A., Guerrini, M., and Focher, B. (1991). Inclusion complexes of
636 bioprime with β -Cyclodextrin in solution and in solid state. *International Journal of*
637 *Pharmaceutics*, 77, 247–254. [https://doi.org/10.1016/0378-5173\(91\)90323-G](https://doi.org/10.1016/0378-5173(91)90323-G).
- 638 [37] Mura, P. (2015). Analytical techniques for characterization of cyclodextrin complexes in the solid
639 state: A review. *Journal of Pharmaceutical and Biomedical Analysis*, 113, 226–238.
640 <https://doi.org/10.1016/j.jpba.2015.01.058>.
- 641 [38] Zarif, M.S., Afidah, A. R., Abdullah, J. M., and Shariza, A. R. (2012). Physicochemical
642 characterization of vancomycin and its complexes with β -cyclodextrin. *Biomedical Research*
643 *(India)*, 23, 513–520.
- 644 [39] Sapte, S., and Pore, Y. (2016). Inclusion complexes of cefuroxime axetil with β -cyclodextrin:
645 Physicochemical characterization, molecular modeling and effect of L-arginine on complexation.
646 *Journal of Pharmaceutical Analysis*, 6, 300–306. <https://doi.org/10.1016/j.jpba.2016.03.004>.
- 647 [40] Birks, J. B. (1970). *Photophysics of aromatic molecules*, Wiley-Interscience, London,
648 <https://doi.org/10.1002/bbpc.19700741223>.

- 649 [41] Sameena, Y., Sudha, N., Chandrasekaran, S., and Enoch, I. V. M. V. (2014). The role of
 650 encapsulation by β -cyclodextrin in the interaction of raloxifene with macromolecular targets: a
 651 study by spectroscopy and molecular modeling. *Journal of Biological Physics*, 40, 347–367.
 652 <https://doi.org/10.1007/s10867-014-9355-y>
- 653 [42] Kano, K., Takei, M., and Hashimoto, S. (1990). Cationic porphyrins in water: proton NMR and
 654 fluorescence studies on dimer and molecular complex formation. *Journal of Physical Chemistry*,
 655 94, 2181–2187. <https://doi.org/10.1021/j100368a082>.
- 656 [43] Reis, T. A., Jaculi, A. E., Ramos, K. L. V., Souza, P. E. N., Veiga-Souza, F. H., Joanitti, G. A.,
 657 Azevedo, R. B., Gratieri, T., Cunha-Filho, M., and Gelfuso, G. M. (2019). Combination of
 658 cyclodextrin complexation and iontophoresis as a promising strategy for the cutaneous delivery of
 659 aluminum-chloride phthalocyanine in photodynamic therapy. *European Journal of*
 660 *Pharmaceutical Sciences*, 139, 105056. <https://doi.org/10.1016/j.ejps.2019.105056>.

661 **Graphical Abstract (dimension 13 cm x 5 cm)**



662

663

664